Experimental study of the behavior of confined variable density jets in a time varying crossflow

Nathalie Raud, Yannick Bury, Rudy Bazile, Jacques Borée, Georges Charnay

N. Raud[1]
Ph.D.

Y. Bury
Ph.D. Student.

R. Bazile
Assistant Professor.

J. Borée
Research Scientist.

G. Charnay
Research Director.

Institut de Mécanique des Fluides de Toulouse, UMR CNRS/INPT-UPS 5502, Avenue Camille Soula, 31400 Toulouse, France

Experimental Study of the Behavior of Confined Variable Density Jets in a Time Varying Crossflow

An experimental work and a physical analysis dedicated to the study of a low density jet subjected to a time varying crossflow with high acceleration/deceleration levels are presented in this paper. Relevant nondimensional numbers are derived and show that unsteady effects associated with the presence of the jet in the acceleration field have noticeable consequences on the flapping of the jet. The Schlieren technique is applied in the test section of a square duct to obtain time resolved images of the jet. Analysis of the results is focused on the influence of the unsteady effects on the global dynamic behaviour of the jet in the near field. The interaction between the jet and the crossflow is analysed in three contrasted situations corresponding to different values of the jet outlet velocity U_0. We predict and observe an increase of the jet deflection during the acceleration phase and a competition between drag and acceleration during the deceleration. This competition is particularly clear for the two lowest ejection velocities of the jet and we have shown that the jet is initially deflected upstream the nozzle. The influence of exit jet injection angle is finally considered. We show that upstream or downstream injections induce a very strong modification of the mixing process of the jet fluid with the pulsed crossflow.

1 Introduction

The flow associated with the turbulent mixing of a jet exhausting at large angles in a crossflow is an example of complex three-dimensional shear flows. This situation is widely used in many technical applications where efficient mixing of the jet fluid with the surrounding is of primary importance (Broadwell and Breidenthal, 1984; Smith and Mungal, 1998). Applications include such contrasted practical problems as discharge of waste gases from chimney stacks, control of missiles or aircraft, gas turbine combustor cooling, or fuel injection. One can refer to the review of Margason (1993) for a complete literature survey concerning jets in crossflow. The crossflow modifies the direction of the initial momentum flux of the jet and three-dimensional effects are important. For nonconfined situations, the structure of the flow is known to range from a free jet like behavior in the near field to a counter-rotating vortex pair in the far field (Kamotani and Greber, 1972; Keffer and Baines, 1963). Typical vortex systems associated with the crossflow interaction are now well-identified (Kelso, Lim, and Perry, 1996). Moreover, the instantaneous structure of the flow bears only a little resemblance to ensemble averaged velocity fields (Smith, Lozano, Mungal, and Hanson, 1993).

In the far field of the jet, Broadwell and Breidenthal (1984) have considered the jet as a point source of normal momentum and have shown that the only global length scale is rD_0. r is the square root of the momentum flux ratio $r = (\rho_0 U_0^2/\rho_1 U_1^2)^{1/2}$. Here, U is velocity, ρ is density, and subscript 0 and 1 refer to jet properties and crossflow properties, respectively. In the near field, Smith and Mungal (1998) have recently shown that the vortex interaction region displays a D_0 scaling which allows for structural effects that depend on the ratio r. Finally, a third length scale $r^2 D_0$ can be used to collapse the data in the first diameter from the jet exit and to locate the branch point of the counter-rotating vortex pair (Smith and Mungal, 1998).

Turbulent jets in confined crossflow are relevant configurations for a lot of engineering situations but have received considerably less attention than turbulent jets in unbounded crossflows (Catalano et al., 1989; Kamotani and Greber, 1974; Stoy and Ben-haim, 1973). Catalano et al. (1989) have shown that the existence of impingement on the opposite wall is strongly dependant on the jet to crossflow velocity ratio r. Stoy and Benhaim (1973) have used a classical one-dimensional analysis and concluded that the jet trajectory and impingement point can be fairly well predicted using correlations derived in unbounded flows. However, no systematic study of the effect of confinement seems available in the literature.

To the authors' knowledge, no studies are reported concerning the effects of a pulsed crossflow on a jet. Practical applications corresponding to this situation are, however, quite common. For example, the present work is directly linked with the development of natural gas vehicles (NGV) which have a high potential to reduce urban air pollution (Stephenson, 1997). In such spark ignition engines, the gaseous fuel, significantly lighter than the surrounding air ($\rho_0/\rho_1 = 0.5$), is injected in intake ports and submitted to a pulsed air flow where acceleration can reach values of 3000 g (Bates, 1989) – g is the gravity acceleration field. A knowledge of the mixing process of the jet in this particular unsteady situation is clearly useful to optimise the combustion.

In this paper, we will focus on the description of the global behavior of a confined variable density jet in a periodic crosswind. A first physical analysis will show that the unsteady effects associated with the presence of the jet in the acceleration field are expected to have noticeable consequences on the flapping of the jet which are of course enhanced in the case of jets significantly lighter than the ambient fluid. Time resolved images of the near field of a light heated jet ($\rho_0/\rho_1 = 0.5$) have

[1] Present Address: Siemens Automotive SA, Toulouse, France.

Contributed by the Fluids Engineering Division for publication in the JOURNAL OF FLUIDS ENGINEERING. Manuscript received by the Fluids Engineering Division March 6, 1998; revised manuscript received September 21, 1998. Associate Technical Editor: S. Banerjee.

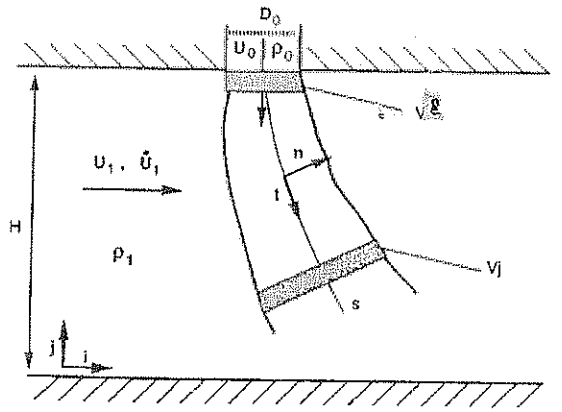

Fig. 1 Jet configuration

been obtained by Schlieren technique in a model experiment setup. In the case of a jet directed normally to the crossflow, contrasted situations corresponding to different values of the ratio of the unsteady effects to the jet initial momentum flux will be presented and discussed. A comparison of the relevant time scales in this situation provides an understanding of the important physical mechanisms.

The behavior of non-normal jets will be described in the last part. We will specifically show that a slight counterflow injection induces dramatic changes and a better dispersion of the injected fluid in the crossflow even during the acceleration phases. Such configurations could have interesting applications in practical situations.

2 Physical Analysis and Derivation of Relevant Nondimensional Numbers

We consider the situation presented in Fig. 1. The jet fluid has an ejection velocity U_0 and an initial density ρ_0 eventually very different from the ambient density ρ_1. In this first part, we assume that the jet flows perpendicularly to the time varying crossflow $U_1(t)$. We will focus on the dynamical behavior of the flow in the first diameters of the jet. The initial momentum flux of the jet can be affected by gravity effects and by the uniform transversal flow of speed U_1 varying with time ($\dot{U}_1 = dU_1/dt$). The time scale of the pulsation classically defined as $\tau_{U_1} \approx \min(U_1/\dot{U}_1)$ is an important quantity that has to be compared with the other relevant time scales. The effect of the gravity field $\mathbf{g}$ is neglected in all the cases presented in this paper. First, it can be easily checked that the jet Froude number defined by $F_j = \rho_0 U_0^2/g|\rho_0 - \rho_1| D_0$ (Chen and Rodi, 1980) is significantly large. The initial development of the jet is therefore inertial and is not affected by gravity (Chassaing et al., 1994; Panchapakesan and Lumley, 1993). Second, we deal with contrasted situations with $|\dot{U}_1| \gg g$ and $\tau_{U_1} \ll \tau_g$ where τ_g is the characteristic time scale of the movement induced by gravity over the channel height H (Tritton, 1988).

A large amplitude pulsation of the crossflow is expected to have a significant effect on the jet behavior. An integral model describing the time and space evolution of the far field of the unsteady jet submitted to a time varying crosswind has been established in (Raud, 1997). A simplified analysis is presented here in order to focus on the flow behavior at the jet outlet and to derive relevant nondimensional numbers. Let us consider the control volume V_c of thickness $\Delta s \ll D_0$ and limited by the jet contour drawn in Fig. 1 at the exit of the fixed jet nozzle of surface S_0. We can easily show (Raud, 1997) that the inertia effects due to the movement of the control volume are negligible. We further assume that the velocity profile is uniform of velocity $\mathbf{V} = U\mathbf{t}$ where the vector $\mathbf{t}$ is the local tangent to the jet axis. Finally, we neglect the entrainment of the external fluid by the early developing annular mixing layers. The modulus of $\mathbf{V}$ is therefore constant and equal to the ejection velocity U_0. The mass flux $\mathbf{Q}$ and the momentum flux $\mathbf{J}$ are respectively $\mathbf{Q} = \rho_0 U_0 S_0 \mathbf{t} = Q_0 \mathbf{t}$ and $\mathbf{J} = \rho_0 U_0^2 S_0 \mathbf{t} = J_0 \mathbf{t}$. The momentum balance writes:

$$\frac{\partial \mathbf{Q}}{\partial t} + \frac{\partial \mathbf{J}}{\partial s} = \frac{J_0}{D_0}\left[\frac{\partial \alpha}{\partial t^*} + \frac{\partial \alpha}{\partial s^*}\right]\mathbf{n} = (\sum F)\mathbf{n} \qquad (1)$$

α is the local angle of the jet axis and $\mathbf{n}$ is the local normal to the jet axis. t^* and s^* are nondimensional time and length based on the jet scales with $t^* = tU_0/D_0$ and $s^* = s/D_0$. ΣF represents the sum of the normal forces by unit length applied on the fluid contained in V_c by the external flow. Near the jet outlet, we have therefore:

$$\left[\frac{\partial \alpha}{\partial t^*} + \frac{\partial \alpha}{\partial s^*}\right] = \sum\left(\frac{D_0 F}{J_0}\right) \qquad (2)$$

In Eq. (2), nondimensional numbers $N = D_0 F/J_0$ represent the spatio-temporal change of α. $N = D_0/L$ compares the steady jet length scale to the characteristic length $L = J_0/F$ associated with the force F. If $N \ll 1$, force F has only a little effect on the exhaust flow. On the contrary, if $N \gg 1$, the exhaust flow is significantly influenced by the external unsteadiness. Neglecting possible history effects, F is classically decomposed into three terms with $\Sigma F = F_D + F_I + F_M$. F_D denotes the quasi-steady drag, F_I represents the pressure force applied by the outer flow to accelerate the equivalent volume V_e of external fluid and F_M is the added mass force due to the presence of the jet in the acceleration field.

The following expressions are easily obtained:

$$F_D = C_d \tfrac{1}{2} D_0 \rho_1 U_1^2; \quad F_I = S_0 \rho_1 \dot{U}_1; \quad F_M = S_0 C_m \rho_1 \dot{U}_1 \qquad (3)$$

F_D is positive as the crossflow is always in the positive direction in the present work.

C_d is the equivalent aerodynamic drag coefficient between crossflow and jet. We assume that the value of C_d is of the same order of magnitude as the value of the drag coefficient of a rigid cylinder (Adler and Baron, 1979; Ooms, 1977). The mean value of the equivalent Reynolds number $R_e = (\bar{U}_1 D_0/\nu)$ is of order 2.10^4, we therefore choose $C_d = 1$. Note that assuming a constant value for C_d removes the effect of the crossflow unsteadiness from the drag force term and that no history forces are considered here. The added mass coefficient C_m is fixed at $C_m = 1$ equal to the coefficient of a rigid cylinder.

The final expressions of N_D (drag effect) and N_{acc} (acceleration effects) are:

$$N_D = \frac{D_0 F_D}{J_0} = \frac{2C_d}{\pi}\frac{\rho_1 U_1^2}{\rho_0 U_0^2}$$

$$N_{acc} = \frac{D_0(F_I + F_M)}{J_0} = (1 + C_m)\frac{\rho_1 D_0 \dot{U}_1}{\rho_0 U_0^2} \qquad (4)$$

The expression of N_D is classical. N_{acc} compares the jet momentum flux to the unsteady pressure effects. Note that these unsteady effects are expected to play a role even if the density ρ_0 is equal to the ambient density ρ_1 because the location of the jet exhaust is fixed in the acceleration field. Both drag and unsteady effects are, however, inversely proportional to the density ratio ρ_0/ρ_1 and are therefore enhanced for light jets.

During an acceleration phase, N_D and N_{acc} have the same sign and the acceleration is expected to increase the jet deflection. On the contrary, during a deceleration phase, unsteady effects are opposed to drag effects and can eventually dominate. To illustrate these statements, the ratio N_{acc}/N_D is computed below

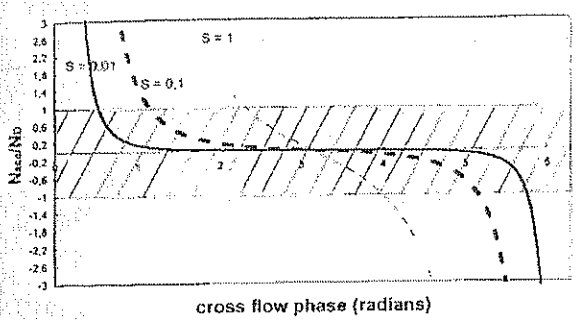

Fig. 2 Evolution of N_{acc}/N_D over a crossflow period for increasing values of parameter $S = D_0 f/U_m$

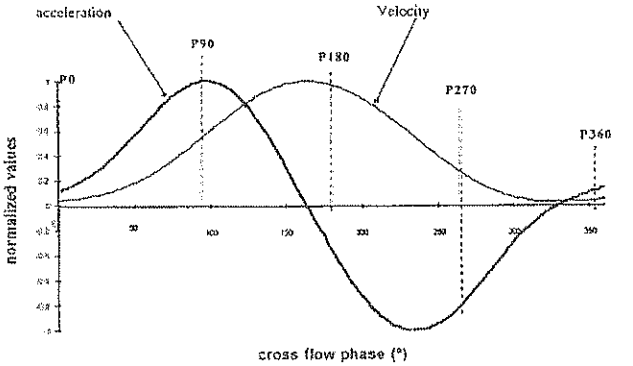

Fig. 4 Evolution of mean velocity and acceleration of the crossflow on the axis of the duct below the jet nozzle (as a function of the phase of the crossflow)

for a periodically time varying crossflow of velocity $U_1(t) = (U_m/2)[1 - \cos(\omega t)]$. One gets:

$$\frac{N_{acc}}{N_D} = \frac{\pi(1 + C_m)}{2C_d}\frac{D_0\dot{U}_1}{U_1^2} = 2\pi^2\frac{1 + C_m}{C_d}\left[\frac{\sin(\omega t)}{1 - \cos(\omega t)}\right]\frac{D_0 f}{U_m} \quad (5)$$

f is the frequency of the pulsation with $f = \omega/2\pi$. N_{acc}/N_D compares the advective time scale D_0/U_1 to τ_{U_1}. The evolution of N_{acc}/N_D is drawn in Fig. 2 for increasing values of the non-dimensional number $S = D_0 f/U_m$. Hatched part of Fig. 2 corresponds to the region of drag effects domination. An increase of S from $S = 0.1$ to $S = 1$ enhances significantly the region of acceleration domination while drag effects are always significant for $\omega t \approx \pi$ corresponding to the maximum crosswind velocity and negligible acceleration. N_{acc}/N_D becomes negative during the deceleration phase. For $N_{acc}/N_D < -1$, the resultant normal force at the jet exhaust is opposed to the flow direction. Corresponding effects will be observed in the following.

Volumes of jet fluid propelled into the pipe flow entrain external air. The resulting mixture experiences the significant velocity and acceleration of the incident flow. Some signatures of the acceleration effects will be observed in the following and a qualitative understanding will be obtained by considering the dynamics of a coherent finite fluid volume in the incident pulsed flow (Hunt, 1987).

3 Experimental Arrangement

3.1 Flows Generation and Main Characteristics

3.1.1 Crossflow. Experiments are performed in a $H = 60$ mm square cross section air tunnel (Fig. 3). The test section is equipped with large windows for the optical access. A fan generates the main crossflow. For the maximum value of the steady crossflow velocity [max $(U_1) \approx 40$ ms^{-1} (± 1 ms^{-1})], the Reynolds number based on the hydraulic diameter is equal to 115,000 and the ratio between the length of the duct L and the half width of the test section is equal to 58. This ensures that the flow is reasonably established at the observation zone (Schlichting, 1979). Velocity measurements have been performed using a hot wire probe (Raud, 1997). Profiles of mean and rms axial velocity are typical of steady fully developed turbulent pipe flow. An integral time scale of the turbulence, τ_t, can be estimated by the ratio h/u^*, where the friction velocity, u^*, is derived from the Blasius relation ($u^* = 0.96$ ms^{-1}). The value of τ_t is approximately 30 ms.

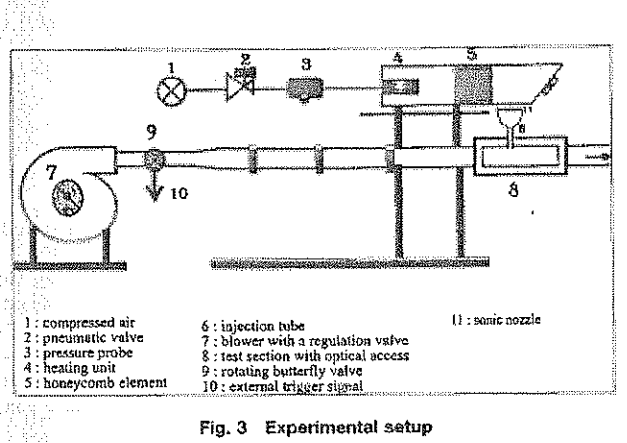

Fig. 3 Experimental setup

A rotating butterfly valve located two meters upstream of the test section produces velocity modulations of the main air flow. Previous studies have shown that rotating butterfly valves can be used to generate quasi-sinusoidal modulations of the velocity in a square duct (Charnay and Mathieu, 1976). A periodic time variation of U_1 is obtained in the present duct for a frequency $f = 66$ Hz (± 0.5 Hz). Figure 4 shows the evolution of the mean velocity on the axis of the test section (averaged from one hundred cycles), as a function of the angle of the rotating value. The velocity amplitude varies from $U_1 = 1.2$ ms^{-1} to a maximum value of $U_1 = 42$ ms^{-1}. The quasi-sinusoidal acceleration curve obtained by time derivation of the measured velocity evolution is superimposed in Fig. 4. The unsteadiness in the duct can lead to strong values of acceleration up to 506 g with $g = 9.81$ ms^{-2}. Four particular phases (P0, P90, P180, and P270) will be studied in this work and have been added on the graph. These observation phases, regularly spaced over a period of pulsation, cover a wide range of acceleration values (see Table 1) where the unsteady effects can be clearly identified and analysed.

The characteristic time, $\tau_{U_1} \approx \min(U_1/\dot{U}_1)$ of the variation of velocity is equal to $\frac{1}{2}\pi f$ for a sinusoidal evolution (i.e., $\tau_{U_1} \approx 2.4$ ms). τ_{U_1} is much smaller than the integral characteristic time of the turbulence ($\tau_t \approx 30$ ms estimated under steady conditions). The turbulence is therefore not established under unsteady conditions.

3.1.2 Jet. The heated air jet [$T_0 = 550$ K (± 2 K), $\rho_0/\rho_1 = 0.5$] is injected through a cylindrical tube ($D_0 = 14$ mm) into the main crossflow with an angle of 90 deg (except in Section 4.3 where the influence of the jet angle is presented). The confinement of the jet is important in this study with $H \approx 4D_0$ (see Fig. 1). Jet impingement can therefore occur during the unsteady flapping of the jet and will be analysed in the following section.

The use of a sonic nozzle ensures a jet of constant mass flux. This sonic nozzle is located just before the convergent section

Table 1 Crossflow velocities and acceleration values at the four selected phases. Expressions of P, N_{acc} and N_D for the three exit jet velocities cases. (Uncertainty of N: 10%.)

		P0		P90		P180		P270	
U_t (m.s^{-1})		2		22		40.5		9.5	
$\dot{U}_t$ (m.s^{-2})		70 g		500 g		-180 g		-380 g	
	P	N_D	N_{acc}	N_D	N_{acc}	N_D	N_{acc}	N_D	N_{acc}
Case 1 : U_0=56 m s^{-1}	0.4	$1.6\ 10^{-3}$	$1.2\ 10^{-2}$	0.20	$9\ 10^{-2}$	0.66	$-3.1\ 10^{-2}$	$3.7\ 10^{-2}$	$-6.6\ 10^{-3}$
Case 2 : U_0=39 m s^{-1}	0.65	$3.3\ 10^{-3}$	$2.5\ 10^{-2}$	0.41	0.18	1.4	$-6.5\ 10^{-2}$	$7.6\ 10^{-2}$	-0.14
Case 3 : U_0=14 m s^{-1}	1.6	$2.6\ 10^{-2}$	0.2	3.1	1.4	10.7	-0.50	0.59	-1.1

of the injection device (see Fig. 3). The volume within the convergent and the tube damps any acoustic perturbation induced by the sonic aperture. It has been chosen small enough so that the pressure and related density time variations in the duct, induced by the pulsed crossflow, have no significant influence on the jet exit velocity (small variations less than 1 percent have been estimated (Borée, 1990)).

The exit jet velocity can be set from $U_0 = 10$ ms^{-1} to $U_0 = 60$ ms^{-1} for Reynolds numbers contained between 8900 and 53,500. The uncertainty of the velocity U_0 is 3 percent. Velocity measurements have ensured that the velocity profile at the outlet of the nozzle is nearly uniform for the different operating conditions (Raud, 1997). The maximum turbulence intensity on the axis of the jet is 2 percent.

3.2 Imaging System. In order to observe the jet as it interacts with the main flow, the Schlieren technique was used and adapted to unsteady conditions. The density gradients due to the presence of the heated jet are detected with a gated CCD camera. The integration time of the camera is chosen short enough (40 μs) compared to the period of the crossflow velocity ($2\pi/\omega = 15$ ms) in order to obtain time-resolved images of the heated jet at a given phase ωt. An external signal provided by the rotating butterfly valve (with an accuracy of 1 deg) is used to synchronize the imaging system. The video signal is digitized by a frame grabber board (Magic MATROX, 768 × 572 pixels, 8 bits) connected to a PC. A specific image processing was developed to extract the instantaneous jet boundary in a selected window that corresponds to a field of view of 60 mm height by 85 mm length.

The Schlieren technique is suitable to analyze the location and the global structure of the jet as it interacts with the pulsed crossflow, but no information will be obtained concerning the well known 3D effects and the vortex structures that appear in the present configuration (Kamotani and Greber, 1972).

3.3 Post-Processing. Some Schlieren images dedicated to a pure descriptive approach will be presented in the next section without post-treatment. On the other hand, a more precise and objective analysis of the jet structure for different operating conditions requires a particular post-processing to extract the jet boundary. Images obtained from the Schlieren technique cannot be directly interpreted in terms of pixel value. Moreover, a local pixel value in the jet can be the same than in the background, so that a systematic threshold on the grey levels cannot be easily applied to extract the jet from the background of the image.

The algorithm of the processing is based on the following observation: considering a zoom on a small test window (in the background or in the jet), it appears that the background is locally homogeneous contrary to the heated jet where the density gradients lead to a strong dispersion of the pixel values. The post-processing can be described in two steps. First, over a small test window (11 × 11 pixels) the root mean square of the pixel values is calculated and provides the information concerning the local homogeneity of the image. A small value of this rms, is obtained when the processing window is located in the background whereas high values are expected in the jet.

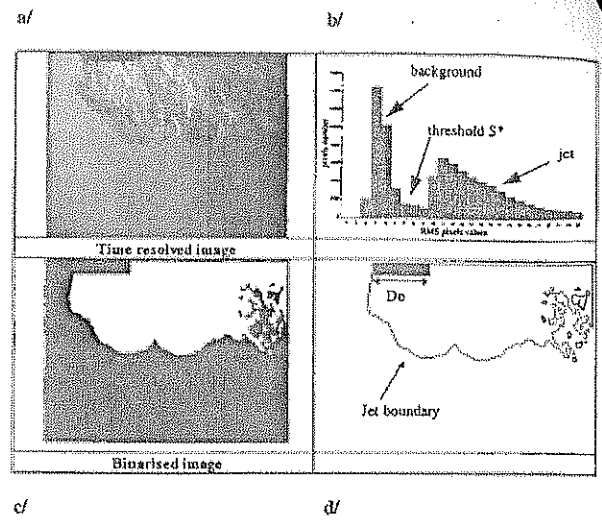

Fig. 5 (a) Typical instantaneous Schlieren image of the jet in the pulsed crossflow (b) Typical histogram of all the RMS pixels values computed in the test window (11 × 11 pixels) when moving on the whole image. S^* is a threshold between the jet and the background contributions. (c) Binarization of the jet image (5.a) after the post-processing. (d) Jet boundary extracted after application of a sobel gradient on 5.c.

Figure 5(a) shows a typical histogram of all the rms, pixels values obtained when the test window is moved (pixel by pixel) over the whole image. A cut-off level, S^*, can be objectively determined at the dip between the contribution of the homogeneous background (rms pixel values smaller than S^*) and the contribution of the jet (rms pixel values higher than S^*). When the test window contains jet and background contributions, there is some overlap of the histograms; but the number of calculated values corresponding to this particular case remains negligible and the dip at S^* is still marked. In a second step, when S^* is known, the processing window is moved again over the whole image and its central pixel is replaced by 0 if S^* is not reached (background). Then a simple threshold of the grey levels can extract easily the jet boundary (Fig. 5(b/c/d)).

4 Results and Discussion

Topologic information will be extracted from instantaneous images at a given phase and analysed in terms of global behavior of the jet and mixing between the hot air and the pulsed crossflow. A limited set of images were acquired during the study in each configuration considered. This set is not large enough to perform a precise phase averaging but ensures that the images presented here are fully representative of the periodic evolution of the flow and adapted to the following discussion focused on three points. First, the interaction between the jet and the pulsed flow is analysed for a jet with high ejection velocity corresponding to an important ejection momentum flux and low values of the non-dimensional numbers N. Then the influence of the jet ejection velocity is considered. Lower ejection velocities correspond to a more pronounced interaction with the pulsed crossflow. Finally, results with a variable ejection angle are presented and discussed in terms of influence of the injection concept on the mixing process.

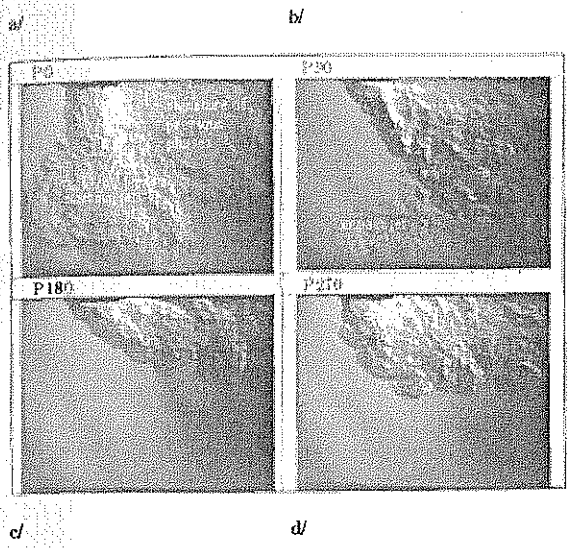

Fig. 6 Time resolved images of the jet (high velocity case: U_0 = 56 m.s^{-1}) at the selected phases of the pulsed crossflow

4.1 Analysis of the Dynamic Behavior of the Jet. Instantaneous images of the heated jet (ejection velocity: 56 ms^{-1}) are presented in Fig. 6 at the different observation phases defined in Section 3. This sequence shows how the acceleration field of the pulsed crossflow perturbs the jet. The jet varies from a straight jet at P0 to a completely deflected jet at P180. The flapping of the jet is a time-continuous periodic phenomenon and the distribution of hot air observed at a given phase inherits the events that occur at the previous phases. These history effects are clearly visible in Figs. 6(a–d). At P0 (Fig. 6(a)), both the crossflow velocity and acceleration are small, the jet penetrates across the main flow and behaves like a starting jet in a quiescent surrounding (Witze, 1980). In particular, the transient vortex region heading the jet is well detected in Fig. 6(a). A hot mixture is also detected at P0 downstream of the starting jet but along the upper half of the channel only. This mixing configuration is the signature of the previous phases. Large pockets of unmixed incident fluid therefore flow downstream of the injection point along the channel lower wall.

The jet impacts on the channel lower wall between phases P0 and P90. To analyze this point, let us introduce a characteristic time defined as: $\tau_j = H/U_0$. τ_j represents the time needed for the jet fluid to cross the height of the duct with velocity U_0. With $H \approx 4D_0$, note that U_0 is a correct velocity scale in the potential core of the jet. Considering τ_{U_1}, the characteristic time of variation of velocity ($\tau_{U_1} = \frac{1}{2}\pi f$), the ratio $P = \tau_j/\tau_{U_1}$ can be used to estimate the relative distance covered by the jet fluid through the duct. In other words a value of $P < 1$ corresponds to a jet that can reach and impact the lower wall. This is consistent with the present case where τ_j = 1 ms, τ_{U_1} = 2.4 ms and P = 0.4. Hot air pockets, witness of this impact, are convected and accelerated downstream along the lower wall at P90 (Fig. 6(b)). At the phase P90, the external velocity U_1 increases and the acceleration is maximal. The core of the jet is strongly deflected. An objective way to isolate the unsteady effects is to compare Fig. 6(b) to the steady situation corresponding to the same velocity of the crossflow. Boundaries of the steady jet (U_1 = 22 ms^{-1}; $\dot{U}_1 = 0g$) and of the unsteady jet (P90: U_1 = 22 ms^{-1}; $\dot{U}_1 = 500g$) are presented respectively in Figs. 7(a) and 7(b). Compared to the steady case, the spreading of the jet is strongly affected by the pulsed crossflow. The non-dimensional numbers N_D and N_{acc} derived in Section 2 are both positive at P90 and are respectively N_D = 0.20 and N_{acc} = 0.09 (see Table 1). Acceleration effects are therefore expected to be significant and to increase the initial deflection of the jet. A zoom of the jet boundary near the nozzle outlet is drawn in Fig. 7(c). The deflection of the unsteady jet is more pronounced and the contribution of the acceleration effects compared to the drag effects is clearly visible on the boundary extractions.

The unsteady jet fluid is strongly deflected and confined near the upper wall at P180 (Fig. 6(c)). With $N_D \approx 0.66$, this strong deflection in the first jet diameter was expected from dimensional analysis. The deceleration is nearly maximum at P270 (Fig. 6(d)). Drag and acceleration effects at the jet outlet are moderate ($N_D \approx 0.04$, $N_{acc} \approx -0.07$) and compete with each other. This may explain why the jet exits perpendicularly in the first diameter and penetrates easier in the flow. One sees that the hot mixture is confined in the upper half of the channel at P270. A precise understanding of the dynamic of the turbulent interface is difficult. Indeed, deceleration induces a strong positive baroclinic torque, which competes with the shear induced by the jet flow. More work is presently dedicated to this aspect which is expected to have a strong influence on mixing.

In the case analyzed in this part, only the penetration of the starting jet type flow at about P0 and the related impact on the lower wall ensures an initial mixing throughout all the channel while large volumes of unmixed incident fluid flow in the channel lower half during the flapping of the jet.

4.2 Influence of the Exit Jet Velocity. The influence of a decrease of the jet ejection velocity is now discussed. Three contrasted cases corresponding respectively to U_0 = 56 ms^{-1}, U_0 = 39 ms^{-1}, and U_0 = 14 ms^{-1} have been studied. The first case has been discussed previously. Images obtained by Schlieren technique at phases P0, P90, P180, and P270 in the two last cases are presented in Figs. 8 and 9. Changing the jet exit velocity is expected to have significant effects on the behavior of the jet. First, existence of a jet impact is dependent of the ratio P, which is inversely proportional to U_0. As the exit jet velocity decreases, the penetration of the jet into the duct becomes less important. One sees that the impact of the jet on the lower wall never occurs for the two lowest ejection velocities. In particular, the jet fluid never crosses the lower part of the duct for U_0 = 14 ms^{-1} which is unfavourable in terms of mixing. Second, the jet initial momentum flux $J_0 = \rho U_0^2 S_0$ decreases strongly with U_0. Drag and acceleration effects are therefore expected to be enhanced.

A comparison of the jet boundaries in steady and unsteady crossflow for U_0 = 39 ms^{-1} (respectively, U_0 = 14 ms^{-1}) at P90 is presented in Fig. 10(a) (respectively, 10(b)). The jet

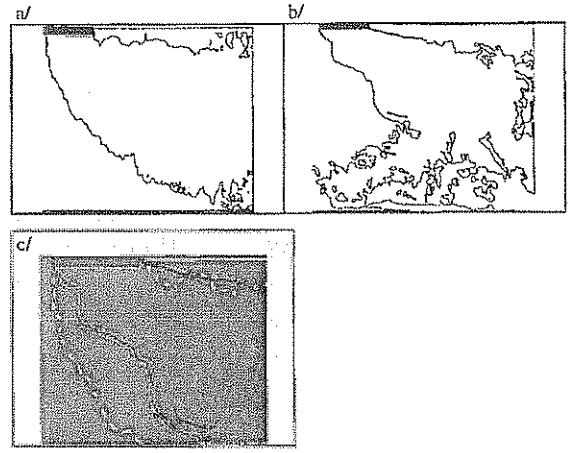

Fig. 7 Jet boundaries (U_0 = 56 m.s^{-1}) extracted respectively for a steady (a) and an unsteady (b) conditions at a phase which corresponds to the same crossflow velocity (U_1 = 22 m.s^{-1}). (c) Comparison of jet boundaries in the first diameters of the jet.

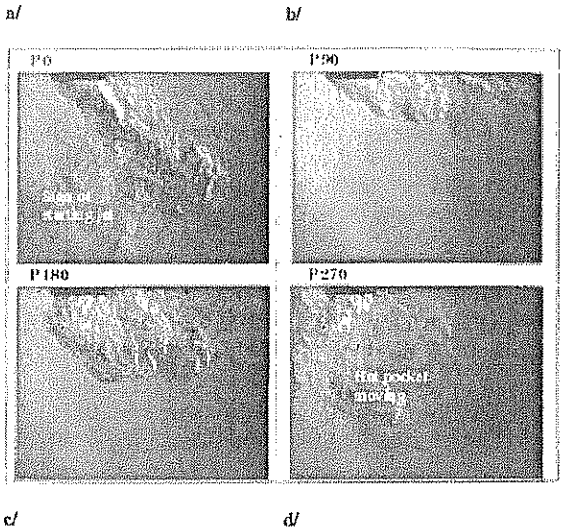

Fig. 8 Time resolved images of the jet (U_0 = 39 ms^{-1}) at the four phases of the pulsed crossflow

is strongly deflected in both cases and the flow of hot mixture develops along the upper wall. The thickness of this layer is, however, significantly reduced in the unsteady situation. This observation is a result of the strong imposed acceleration.

In Figs. 8 and 9, we see that low velocity jets are very sensitive to deceleration. For the sake of clarity, we will focus on phase P270. Table 1 shows that drag and acceleration effects at the jet outlet are significant, opposed and that deceleration effects should dominate. In fact, Figs. 8(d) and 9(d) show that the jet flow is initially deflected upstream the nozzle against the incident flow. One may notice that volumes of jet fluid injected in the channel are moving against the crossflow. This behaviour is believed to be a striking signature of the deceleration effects. A qualitative understanding can be obtained if one considers the dynamics of a coherent finite fluid volume in the incident pulsed flow. Several authors have discussed the motion of such "gas bubbles" in order to investigate either inertia effects in constant density flows (Hunt, 1987) or buoyancy and relative acceleration effects in variable density flows (Chomiak

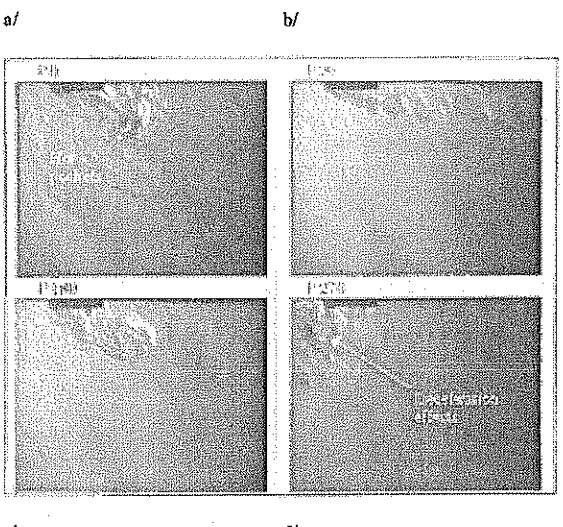

Fig. 9 Time resolved images of the jet (low velocity case: U_0 = 14 ms^{-1}) at the four phases of the pulsed crossflow

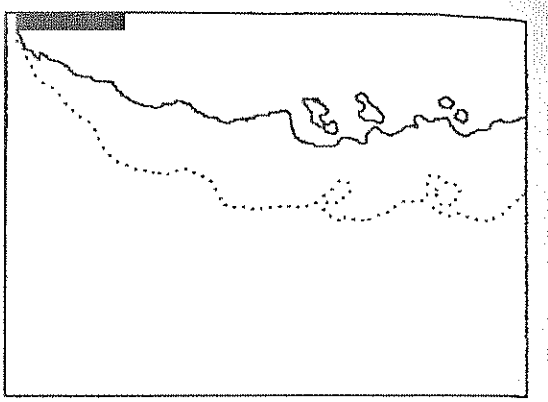

Fig. 10(a)

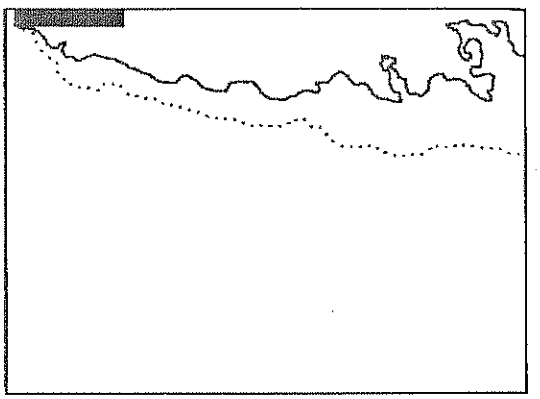

Fig. 10(b)

Fig. 10 Comparison of jet boundaries in steady (---) and unsteady (——) conditions for (a): U_0 = 39 m.s^{-1} and (b): U_0 = 14 m.s^{-1} at P90

and Nisbet, 1995; Veynante and Poinsot, 1997). The simple equations governing the movement of a spherical gas volume submitted to a time varying spatially uniform velocity are recalled in Appendix A and show qualitatively that the unsteady effects due to the external mean pressure gradient and to the added mass force are responsible for such observations. We could proceed in this way by extending the work of (Escudier and Maxworthy, 1973) to take into account entrainment of external air in the gas volume. Any quantitative use of the results would however be very difficult as the particular interaction of the fluid lumps with the time varying external flow depends critically on their unknown initial internal organisations (Chomiak and Nisbet, 1995; Escudier and Maxworthy, 1973).

4.3 Influence of Exit Jet Injection Angle. In this section, we illustrate and compare the behavior of the jet for different injection angles. Varying the jet injection angle can be a sensitive parameter if one wants to optimise the mixing with the crossflow. For example, recent studies (Krothapalli and Shih, 1993; Strykowski et al., 1993) explore the problem of counter current mixing in flows with this goal. Three exit jet angles have been experimented here for an exit jet velocity U_0 = 39 ms^{-1}. Time resolved images at the four phases are presented in Fig. 11 for the downstream injection case (θ = 45 deg) and in Fig. 12 for the upstream injection case (θ = 135 deg). The corresponding phases for a perpendicular jet (θ = 90 deg) were displayed in Fig. 8. For these three cases, the dynamic conditions of the crossflow are similar and equal to the conditions met in the precedent section.

In the downstream injection case (Fig. 11), we again notice a significant deflection of the flow at the jet outlet at phase P90 corresponding to the maximum acceleration. Moreover, the hot

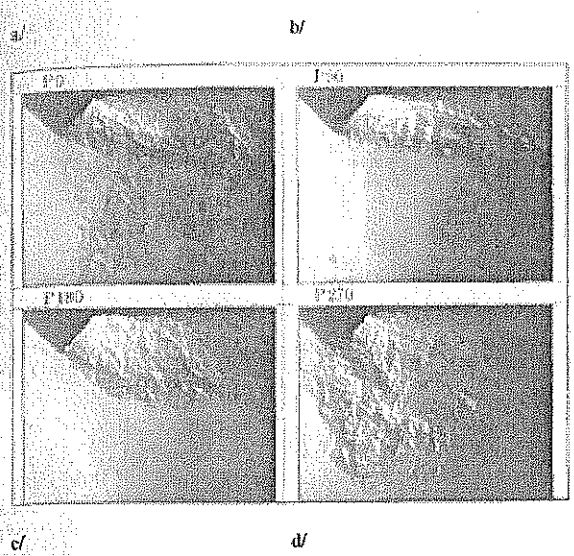

Fig. 11 Instantaneous images of the jet (U_0 = 39 m.s^{-1}) at the four phases of the pulsed crossflow for a jet ejection angle of 45 deg (downstream injection)

mixture is clearly deflected upstream during the deceleration (phase P270). No organized motion is however detected and the turbulent scales involved in this counter-flow are relatively small. By comparing the downstream injection to the perpendicular injection, one may also note that the flapping amplitude of the jet is reduced for the downstream injection.

The structure of the jet is significantly different for upstream injection (Fig. 12). In particular, the jet penetrates completely the duct and impacts on the lower wall about phase P0. As acceleration effects increase, the jet is deflected downstream (phase P90). A large scale turbulent fluid lump of organised nature is clearly seen at phase P180. One sees that this structure flows upstream the jet nozzle during the deceleration phase. In fact, this injection mode is expected to increase the coherence of the large-scale jet fluid lump by increasing the initial vorticity of the structures (Escudier and Maxworthy, 1973). Compared with the two other cases and especially for phases P90 and P180, the major difference is here that the mixture is not confined near the upper wall but expands on the whole height of the duct. This characteristic can be very interesting in terms of homogeneity of the mixing.

Conclusion

An experimental work and a physical analysis dedicated to the study of a low density jet subjected to a time varying crossflow with high acceleration/deceleration levels has been presented in this paper. The crossflow configuration is widely used in many technical applications where efficient mixing of the jet fluid with the surrounding is of primary importance.

A simplified momentum balance was written at the jet exit to derive relevant nondimensional numbers used to estimate the relative importance of the drag and of the acceleration. We have shown that unsteady effects associated with the presence of the jet in the acceleration field are expected to have noticeable consequences on the flapping of the jet which are of course enhanced in the case of jets significantly lighter than the ambient fluid. It was possible to predict an increase of the jet deflection during the acceleration phase and a competition between drag and acceleration during the deceleration; during this phase the unsteady effects can eventually dominate.

The Schlieren technique has been applied in the test section of a square duct to obtain time resolved images of the jet. Analysis of the results was focused on the influence of the unsteady effects on the global dynamic behavior of the jet in the near field and image processing was applied to extract the jet boundary. The modification of the mixing process induced by the unsteadiness was also discussed. The interaction between the jet and the crossflow was analyzed in three contrasted situations corresponding to different values of the jet outlet velocity U_0. The penetration of the hot mixture across the channel is significantly reduced as U_0 decreases. A comparison between jet and pulsation time scales is shown to characterise the possibility of impact of the hot mixture on the lower wall of the channel.

At the phase of maximum acceleration P90 ($\dot{U}_1 = 500\ g$), the influence of the unsteady effects has been isolated by comparing unsteady images to the steady situation corresponding to the same velocity of the crossflow. Compared to the steady case, the spreading of the jet flow submitted to such a strong acceleration is significantly reduced. Conversely, drag and acceleration effects compete with each other at the phase of maximum deceleration P270. This competition is particularly clear for the two lowest ejection velocities of the jet and we have shown that the jet is initially deflected upstream the nozzle as predicted by physical analysis. Moreover, figures display clearly volumes of hot mixture moving against the crossflow in the channel. A qualitative explanation has been proposed.

For the three cases presented here, large volumes of unmixed incident fluid flow in the channel lower half during the flapping of the jet. The influence of exit jet injection angle on the mixing process has been considered. Compared to the perpendicular injection the flapping amplitude is reduced in the downstream injection and the influence of unsteady effects remains quite similar. The most interesting case is the upstream injection where the interaction of the light jet with the crossflow is considerably modified. In particular, over a flapping period, the structure expands on the whole height of the duct and is not confined near the upper wall. Therefore this injection concept provides initial conditions that could be more favourable for the mixing process in terms of spatial homogeneity.

The further evolution of the turbulent mixture carried by the pipe flow should keep a strong memory of the unsteady tridimensional effects observed in the jet near field. Moreover, baroclinic effects and buoyancy driven turbulent scales in the acceleration field are expected to play a significant role in the evolution of this variable density flow.

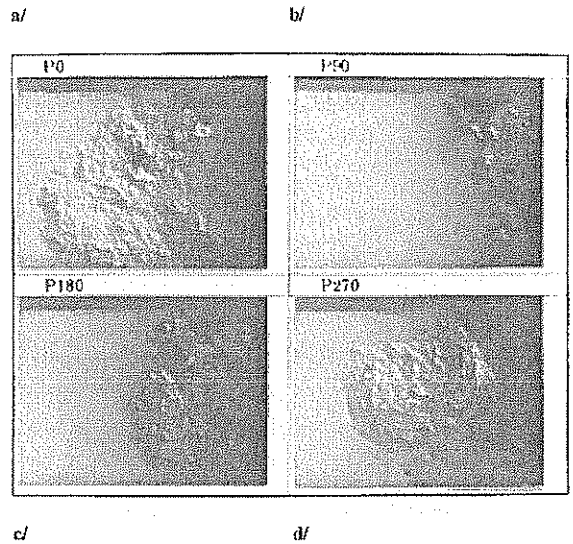

Fig. 12 Instantaneous images of the jet (U_0 = 39 m.s^{-1}) at the four phases of the pulsed crossflow for a jet ejection angle of 135° (upstream injection)

Acknowledgments

This research was supported by the "Conseil Régional de Midi Pyrénées." N. Raud is supported by a grant CIFRE in collaboration with the firm "Energie-Transport-Environnement." We have benefited greatly from discussions with Dr. L. Joly, Dr. H. J. Nuglisch and Dr. P. Labeyrie. The technical support of G. Couteau, J. F. Alquier, and C. Jarnot is acknowledged.

References

Adler, D., and Baron, A., 1979, "Prediction of a Three-Dimensional Circular Turbulent Jet in Crossflow," *AIAA Journal*, Vol. 17, No. 2, pp. 168–174.

Batchelor, G. K., 1967, *An Introduction to Fluid Dynamics*, Cambridge University Press.

Bates, G. J., 1989, "The Effects of Pulsation on Natural Gas Carburation," Thesis University of Auckland.

Borée, J., 1990, "Analyse physique et expérimentale d'un écoulement de jet compressé," Thesis INPT No. 373, Toulouse, France.

Broadwell, J. E., and Breidenthal, R. E., 1984, "Structure and Mixing of a Transverse Jet in Incompressible Flow," *Journal of Fluid Mechanics*, Vol. 148, pp. 405–412.

Catalano, G. D., Chang, K. S., and Mathis, J. A., 1989, "Investigation of Turbulent Jet Impingement in a Confined Crossflow," *AIAA Journal*, Vol. 27, No. 11, pp. 1530–1535.

Charnay, G., and Mathieu, J., 1976, "Periodic Flow in a Wind-Tunnel Produced by Rotating Shutters," ASME JOURNAL OF FLUIDS ENGINEERING, Vol. 98, pp. 1–6.

Chassaing, P., Harran, G., and Joly, L., 1994, "Density Fluctuation Correlations in Free Turbulent Binary Mixing," *Journal of Fluid Mechanics*, Vol. 300, pp. 1–40.

Chen, C. J., and Rodi, W., 1980, "Vertical Turbulent Buoyant Jets—A Review of Experimental Data," HMT-4 Pergamon.

Chomiak, J., and Nisbet, J. R., 1995, "Modeling Variable Density Effects in Turbulent Flames—Some Basic Considerations," *Combustion and Flame*, Vol. 102, pp. 371–386.

Escudier, M. P., and Maxworthy, T., 1973, "On the Motion of Turbulent Thermals," *Journal of Fluid Mechanics*, Vol. 31(3), pp. 541–552.

Hunt, J. C. R., 1987, "Vorticity and Vortex Dynamics in Complex Turbulent Flows," *Transactions of the CSME*, Vol. 11, No. 1, pp. 21–35.

Kamotani, Y., and Greber, I., 1972, "Experiments on a Turbulent Jet in a Cross Flow," *AIAA Journal*, Vol. 10, pp. 1425–1429.

Kamotani, Y., and Greber, I., 1974, "Experiments on Confined Turbulent Jets in a Cross Flow," NASA CR-2392.

Keffer, J. F., and Baines, W. D., 1963, "The Round Turbulent Jet in a Cross-Wind," *Journal of Fluid Mechanics*, Vol. 15, pp. 481–496.

Krothapalli, A., and Shih, C., 1993, "Separated Flow Generated by a Vectored Jet in Crossflow," *AGARD Conference Proceedings 534—Computational and Experimental Assessment of Jets in Crossflow*, pp. 5–1, 5–7.

Margason, R. J., 1993, "Fifty Years of Jet in Crossflow Research," *AGARD Conference Proceedings 534—Computational and Experimental Assessment of Jets in Crossflow*, pp. 1–1, 1–41.

Ooms, G., 1977, "A New Method for the Calculation of the Plume Path of the Gases Emitted by a Stack," *Athmospheric Environment*, Vol. 6, pp. 899–909.

Panchapakesan, N. R., and Lumley, J. L., 1993, "Turbulence Measurements in Axisymmetric Jet of Air and Helium. Part 2. Helium Jet," *Journal of Fluid Mechanics*, Vol. 246, pp. 225–247.

Raud, N., 1997, Mélange Air/Gaz en situation instationnaire. Application à l'emploi du G.N.V. dans les moteurs., Thesis I.N.P. Toulouse N°1316.

Schlichting, H., 1979, *Boundary Layer Theory*, McGraw-Hill, New York.

Smith, S. H., Lozano, A., Mungal, M. G., and Hanson, R. K., 1993, "Scalar Mixing in the Subsonic Jet in Crossflow," *AGARD Conference Proceedings 534—Computational and Experimental Assessment of Jets in Crossflow*, pp. 6–1, 6–13.

Smith, S. H., and Mungal, M. G., 1998, "Mixing, Structure and Scaling of the Jet in Crossflow," *Journal of Fluid Mechanics*, Vol. 357, pp. 83–122.

Stephenson, J., 1997, International Association for Natural Gas Vehicles: A Review of the State of the Art.

Stoy, R. L., and Ben-haim, Y., 1973, "Turbulent Jets in a Confined Crossflow," ASME JOURNAL OF FLUIDS ENGINEERING, Vol. 95, pp. 551–556.

Strykowski, P. J., Krothapalli, A., and Wishart, D., 1993, "Enhancement of Mixing in High-Speed Heated Jets Using a Counterflowing Nozzle," *AIAA Journal*, Vol. 28, No. 12, pp. 2033–2028.

Tritton, D. J., 1988, *Physical Fluid Dynamics*, Oxford Science Publications.

Veynante, D., and Poinsot, T., 1997, "Effects of Pressure Gradients on Turbulent Premixed Flames," *Journal of Fluid Mechanics*, Vol. 353, pp. 83–114.

Wirze, P. O., 1980, The Impulsively Started Incompressible Turbulent Jet. Report no SAND80-8617, Sandia Laboratories energy report.

APPENDIX A

We consider here the movement of a spherical fluid lump of density ρ, volume V and velocity $\mathbf{U}_b$ submitted to a spatially uniform incident flow of velocity $\mathbf{U}_l(t)$ periodically varying with time with $0 \leq U_l(t) \leq U_m$. The density of the ambient fluid is ρ_l.

In a viscous flow, the drag force $\mathbf{F}_D$ non-detailed here is due to the diffusion of vorticity away from the gas volume (Hunt, 1987). A second force is caused by the mean pressure gradient $-\nabla\mathbf{p} = \rho_l\dot{\mathbf{U}}_l(t)$ associated with the acceleration of the external fluid and acting over the volume V. A third force or added mass force is due to the acceleration of the fluid around the spherical body (Batchelor, 1967).

The momentum balance reads:

$$\frac{d\mathbf{U}_b}{dt} = \left[\frac{\rho_l(1 + C_m)}{\rho + C_m\rho_l}\right]\dot{\mathbf{U}}_l(t) + \frac{\mathbf{F}_D}{(\rho + C_m\rho_l)V} \quad \text{(A-1)}$$

In the non-galilean referential linked to the external fluid movement, the evolution of the relative velocity $\mathbf{U}_r = \mathbf{U}_b - \mathbf{U}_l$ is:

$$\frac{d\mathbf{U}_r}{dt} = \left[\frac{\rho_l - \rho}{\rho + C_m\rho_l}\right]\dot{\mathbf{U}}_l(t) + \frac{\mathbf{F}_D}{(\rho + C_m\rho_l)V} \quad \text{(A-2)}$$

In the jet near field, jet fluid volumes propelled in the pipe are partially mixed with the external air and eventually experience a significant initial negative relative velocity with the external flow. In the constant density case ($\rho = \rho_l$), the unsteady pressure effects tend to keep constant this initial relative velocity and a counterflowing fluid lump can clearly be observed during the deceleration phase. Equation (A-2) shows that these effects are enhanced for light fluid ($\rho < \rho_l$) and reduced for heavy fluid ($\rho > \rho_l$) by buoyancy effects induced by the acceleration.